ACS Chemical Neuroscience

pubs.acs.org/chemneuro Research Article

Kinetic Variability in Seeded Formation of ALS-Linked SOD1 Fibrils Across Multiple Generations

Katelyn M. Baumer, Jordan C. Koone, and Bryan F. Shaw*

Cite This: *ACS Chem. Neurosci.* 2020, 11, 304–313 Read Online

ACCESS | Metrics & More | Article Recommendations

ABSTRACT: The unseeded aggregation of superoxide dismutase-1 (SOD1) into amyloid-like fibrils occurs stochastically *in vitro* and *in vivo*, that is, isolated populations of SOD1 proteins (within microplate wells or living cells) self-assemble into amyloid at rates that span a probability distribution. This stochasticity has been attributed to variable degrees of monomer depletion by competing pathways of amorphous and fibrillar aggregation (inter alia). Here, microplate-based thioflavin-T (ThT) fluorescence assays were performed at high iteration (∼300) to establish whether this observed stochasticity persists when progenitor ("parent") SOD1 fibrils are used to seed the formation of multiple generations of progeny fibrils (daughter, granddaughter, and great-granddaughter fibrils). Populations of progenitor fibrils formed stochastically at different rates and fluorescence intensity, however, progeny fibrils formed at more similar rates regardless of the formation rate of the progenitor fibril. For example, populations of progenitor fibrils that formed with a lag time of ∼30 h or ∼15 h both produced progeny fibrils with lag times of ∼8 h. Likewise, populations of progenitor fibrils with high or low maximum fluorescence (e.g., ∼450 or ∼75 A.U.) both produced progeny fibrils with more similar maximum fluorescence (∼125 A.U.). The rate of propagation was found to be more dependent on monomer concentration than seed concentration. These results can be rationalized by classical rate laws for primary nucleation and monomer-dependent secondary nucleation. We also find that the seeding propensity of some "families" of *in vitro* grown fibrils exhibit a finite lifetime (similar to that observed in the seeding of small molecule crystals and colloids). The single biological takeaway of this study is that the concentration of native SOD1 in a cell can have a stronger effect on rates of seeded aggregation than the concentration of prion-like seed that infected the cell.

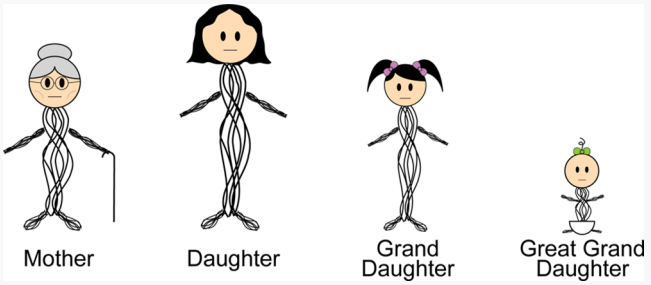

KEYWORDS: *Amyloid, motor neuron disease, amyotrophic lateral sclerosis, superoxide dismutase-1, fibrillation, aggregation, prion*

INTRODUCTION

Approximately 2% of cases of amyotrophic lateral sclerosis (ALS) are caused by >160 different mutations in the gene encoding Cu, Zn superoxide dismutase (SOD1), a homodimeric enzyme.[1−3] Most mutations have an autosomal dominant mode of inheritance, resulting in heterozygous individuals. The self-assembly of mutant and wild-type (WT) forms of SOD1 into amyloid-like oligomers is hypothesized to trigger ALS pathogenesis via a prion-like mechanism.[4−7] Measuring the rate of self-assembly of WT and ALS mutant SOD1 into amyloid-like species—and doing so reliably and reproducibly—is important for: (i) understanding whether mutations induce toxicity by altering intrinsic rates of self-assembly[8,9] or interactions with other proteins[10−12] or membrane surfaces[13−16] and (ii) discovering agents that inhibit or detoxify SOD1 aggregation.

The aggregation of SOD1 into amyloid-like fibrils is stochastic when measured *in vitro*,[17−21] that is, rates of fibril nucleation and propagation span a distribution when measured repeatedly. The aggregation of SOD1 in transgenic ALS-SOD1 mice is also stochastic and follows "test tube" behavior.[22] As an example, when a stock solution of SOD1 is aliquoted into a 96-well microplate and fibrillization in each well is measured simultaneously (via thioflavin-T (ThT) fluorescence), observed rates of fibril nucleation and propagation of iterate wells will often span a bimodal Lorentzian and log-normal distribution, respectively.[17] We previously found that iterate rates of fibril nucleation (expressed as lag time) of WT SOD1 varied by more than 15 h (e.g., from 6 to 22 h); inverse propagation rate constants varied 6-fold (from 1 to 6 h).[17] This stochasticity was attributed to well-to-well variations in the depletion of monomeric SOD1, caused by competing pathways of amorphous and fibrillar aggregation.[17]

Received: August 23, 2019
Accepted: January 2, 2020
Published: January 2, 2020

https://dx.doi.org/10.1021/acschemneuro.9b00464
ACS Chem. Neurosci. 2020, 11, 304–313

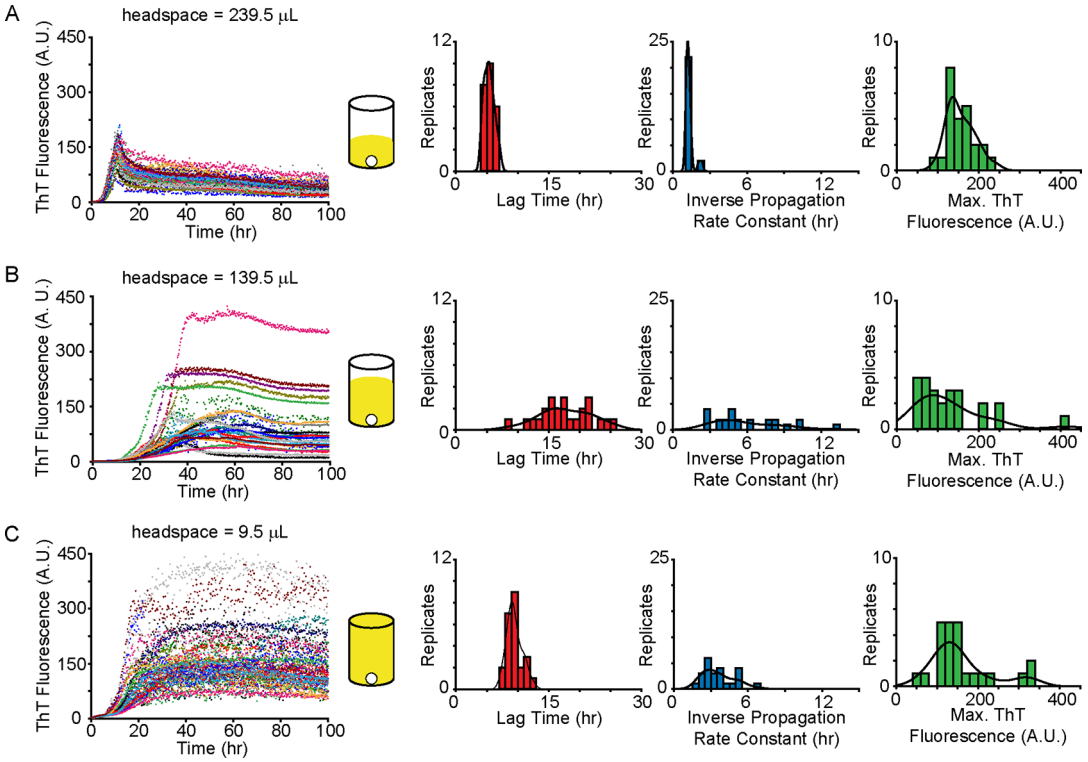

Figure 1. Effect of sample headspace on stochasticity of unseeded fibrillization of apo-SOD1. Solutions of 30 μM apo-SOD1 (per dimer) was incubated with 10 mM TCEP in 10 mM potassium phosphate/5 mM EDTA buffer pH 7.4, and ThT was added to a final concentration of 20 μM. Wells were filled with either (A) 100 μL, (B) 200 μL, or (C) 330 μL of SOD1 aggregation solution. Each well volume was replicated at n = 24, and aggregation was monitored via ThT fluorescence over 5 days. Kinetic parameters of aggregation were determined from sigmoidal curve fits. All assays were carried out in black polystyrene 96-well microplates. The collapse in fluorescence in panel A (at ~10 h) is attributed to adhesion of visible aggregates to the side of microplate wells,[47] proximal to the large air−water interface (this effect is minimized by decreasing headspace).

Previous studies have shown that seeded (templated) fibrillization of other proteins into amyloid is generally less stochastic than unseeded fibrillization.[23−25] In seeded or templated fibrillization processes, a preformed fibril (i.e., a progenitor or parent fibril) is added to a solution of the native, nonfibrillar protein. This exogenously added seed allows the fibrillization process to partially or completely bypass the nucleation step that occurs in unseeded fibrillization, thereby allowing the amyloid state to begin propagating with a shorter lag time. The stochastic nature of SOD1 fibrillization might be caused, in part, by stochastic nucleation. Studies also suggest that the sample headspace (i.e., air−water interface) can contribute to the stochasticity of unseeded amyloid fibrillization (under nonquiescent conditions).[26]

The current study was carried out to answer four questions. First, is the stochasticity of SOD1 fibrillization (observed *in vitro*) an artifact of the sample headspace in microplate wells?[26] Second, is seeded SOD1 fibrillization more, less, or equally stochastic compared to unseeded SOD1 fibrillization? Third, will the *relative* rate of fibrillization observed for one population of SOD1 molecules (i.e., a microplate well exhibiting slow fibrillization versus one exhibiting faster fibrillization) be observed when fibrils from that sample are used to seed the fibrillization of native SOD1? Fourth, does the rate of seeded fibrillization vary across multiple generations of progeny fibrils or is the rate static? Answering these questions will: (i) establish practical guidelines for studying SOD1 fibrillization *in vitro*; (ii) shed light on whether the stochasticity associated with SOD1 fibrillization is caused by fibril polymorphism,[27−32] and (iii) provide kinetic insight into the prion-like propagation of aggregated SOD1 *in vivo*.[33,34] Answering this last question is important for understanding mechanisms of one-hit neuronal cell death.[35] For example, will aggregates that form rapidly in one neural cell seed aggregation in neighboring cells at a faster rate than slow forming aggregates? In this study, WT SOD1 is examined as it is a common denominator in most forms of SOD1-linked ALS.[36]

RESULTS AND DISCUSSION

Stochasticity Associated with Unseeded Fibrillization of SOD1 Persists in Absence of Sample Head Space. The unseeded fibrillization of SOD1 into amyloid-like fibrils occurred stochastically, at a distribution of rates similar to that observed in previous reports.[17] This observed stochasticity did not appear to be entirely caused by the headspace (air−water interface) of the microplate well,[26] as minimizing the headspace did not abolish stochasticity (Figure 1). For example, in the current study (and our previous studies), a standard 96-well microplate was used to perform ThT fluorescence assays of fibrillization. The total capacity of each well is 360 μL; the volume of the sample solution typically added to the well is 200 μL and the Teflon bead occupies ~20.5 μL. Thus, the typical headspace consists of ~139.5 μL of air. This headspace can be effectively removed by filling the sample well to 350.5 μL, leaving a marginal headspace of <10 μL (i.e., solution = 330 μL, bead = 20.5 μL). Decreasing the volume of the headspace from ~140 μL to <10 μL altered the rate of fibrillization of SOD1 but did not entirely abolish stochasticity (Figure 1). Additionally, a larger headspace volume (i.e., ~240 μL of headspace) resulted in more

https://dx.doi.org/10.1021/acschemneuro.9b00464
ACS Chem. Neurosci. 2020, 11, 304−313

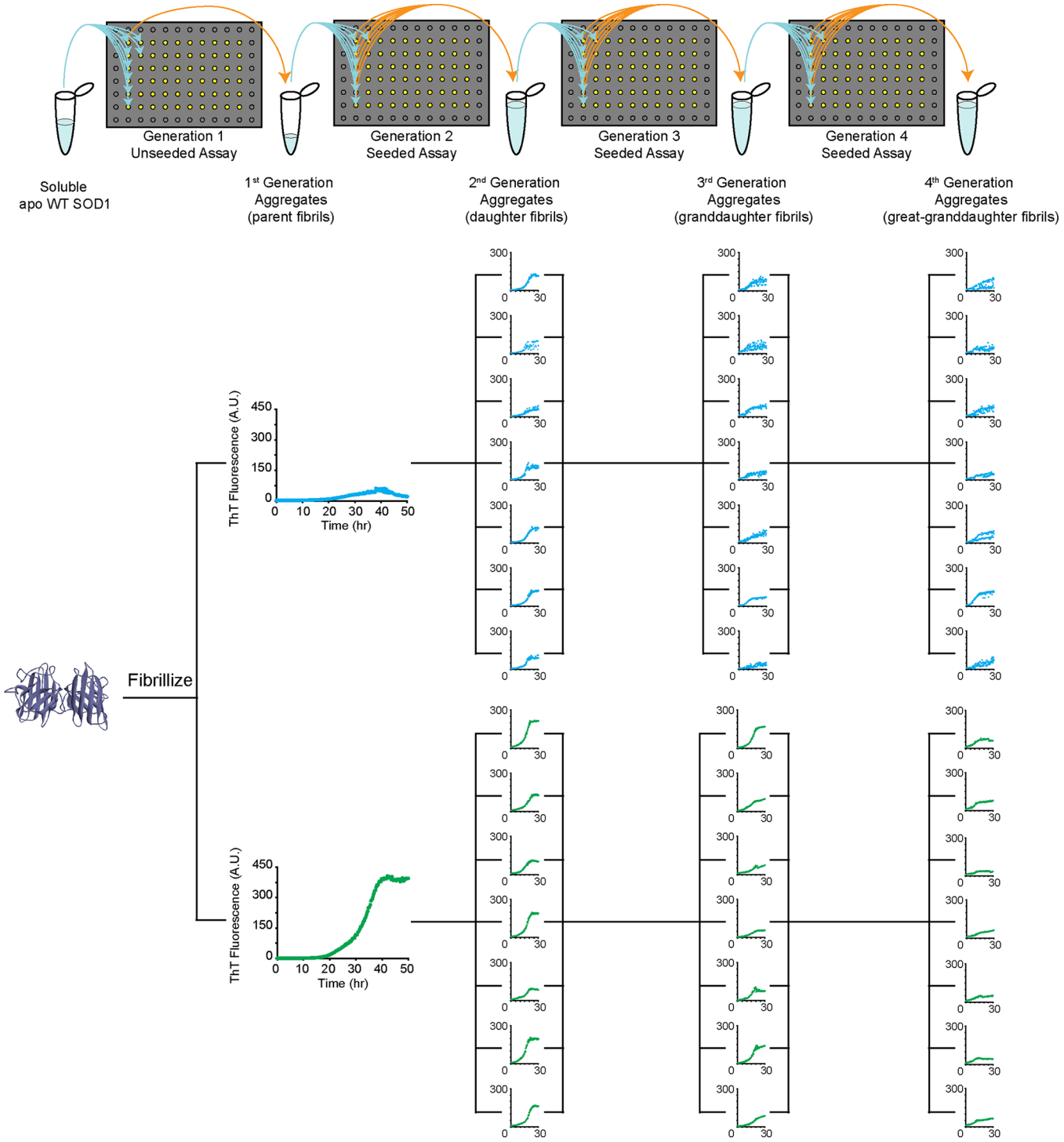

Figure 2. Schematic representation of multigenerational seeded assays. First-generation fibrils (i.e., progenitor or parent fibrils) were prepared from soluble SOD1 without the addition of exogenous seed fibril. Subsequent generations were prepared by addition of seed fibril from one well into seven iterate wells containing soluble SOD1. Subsequent daughter fibrils were then pooled from the seven iterate wells and used to seed granddaughter fibrils. Great-granddaughter fibrils were prepared in the same fashion from granddaughter fibrils.

aggregates adhering to the edges of the well near the air−water interface. Because these aggregates have been effectively removed from the solution, a collapse in ThT fluorescence is observed (Figure 1A). This collapse is more drastic than decreases in ThT fluorescence that are typically observed in these types of assays, which are thought to be caused by quenching of ThT fluorescence upon completion of the elongation phase of aggregation.[37]

SOD1 Progeny Fibrils Form with Shorter Lag Time and Narrower Distributions of Rates than Parent Fibrils. We selected solutions of fibrillized SOD1 from individual microplate wells (formed with our standard headspace of 140 μL) and used these solutions as exogenous "progenitor" seeds to fibrillize second-generation "progeny" fibrils (see Figure 2 for an illustration of this experiment). We wished to determine if fibril seeds from these wells would produce second-

https://dx.doi.org/10.1021/acschemneuro.9b00464
ACS Chem. Neurosci. 2020, 11, 304−313

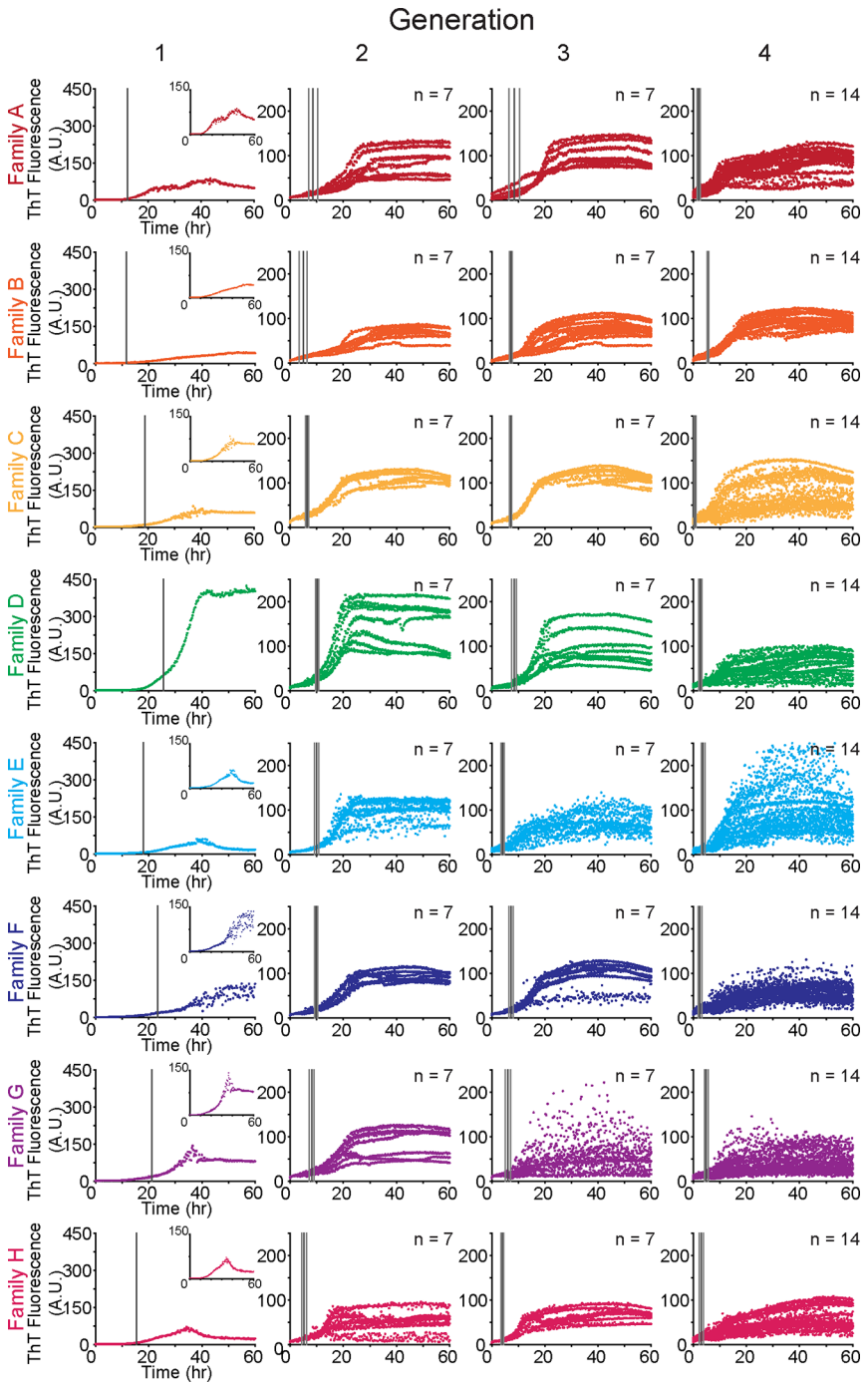

Figure 3. ThT fluorescence of first-generation (parent) and second- to fourth-generation (daughter, granddaughter, and great granddaughter) fibrils. First-generation ThT fluorescence plots are individual replicates from Figure 1B. Each color represents a "family" of fibrils, derived from the same parent seed. Dark gray reference lines in each plot represent the mean lag time, and light gray reference lines represent the standard error of the mean. Sample volumes in all experiments were 200 μL, yielding a headspace volume of ~140 μL.

generation fibrils at the same relative rates (qualitatively) at which the parent seeds formed, that is, fast parents, fast daughters; slow parents, slow daughters. To do so, we selected 8 different progenitor wells that exhibited the full range of fibrillization kinetics, spanning lag times of 11.50 to 25.44 h and inverse propagation rate constants of 2.97 to 10.18 h (Figure 3). These 8 populations of progenitor seeds were used to produce 8 sets of progeny fibrils ("daughters") via a seeded aggregation process (with a headspace of 140 μL). Each progeny generation was formed in replicates of at least seven (Figure 3).

The fibrillization of second-generation SOD1 fibrils exhibited four distinct differences compared to first-generation fibrils. Formation of the second generation of fibrils exhibited less stochasticity than the formation of first-generation unseeded fibrils (Figure 4A). The lag time of second-generation fibrils was, as expected, shorter than first-generation fibrils, and the propagation rates of second-generation fibrils were faster (Figure 4B). For example, the lag time of second-

https://dx.doi.org/10.1021/acschemneuro.9b00464
ACS Chem. Neurosci. 2020, 11, 304−313

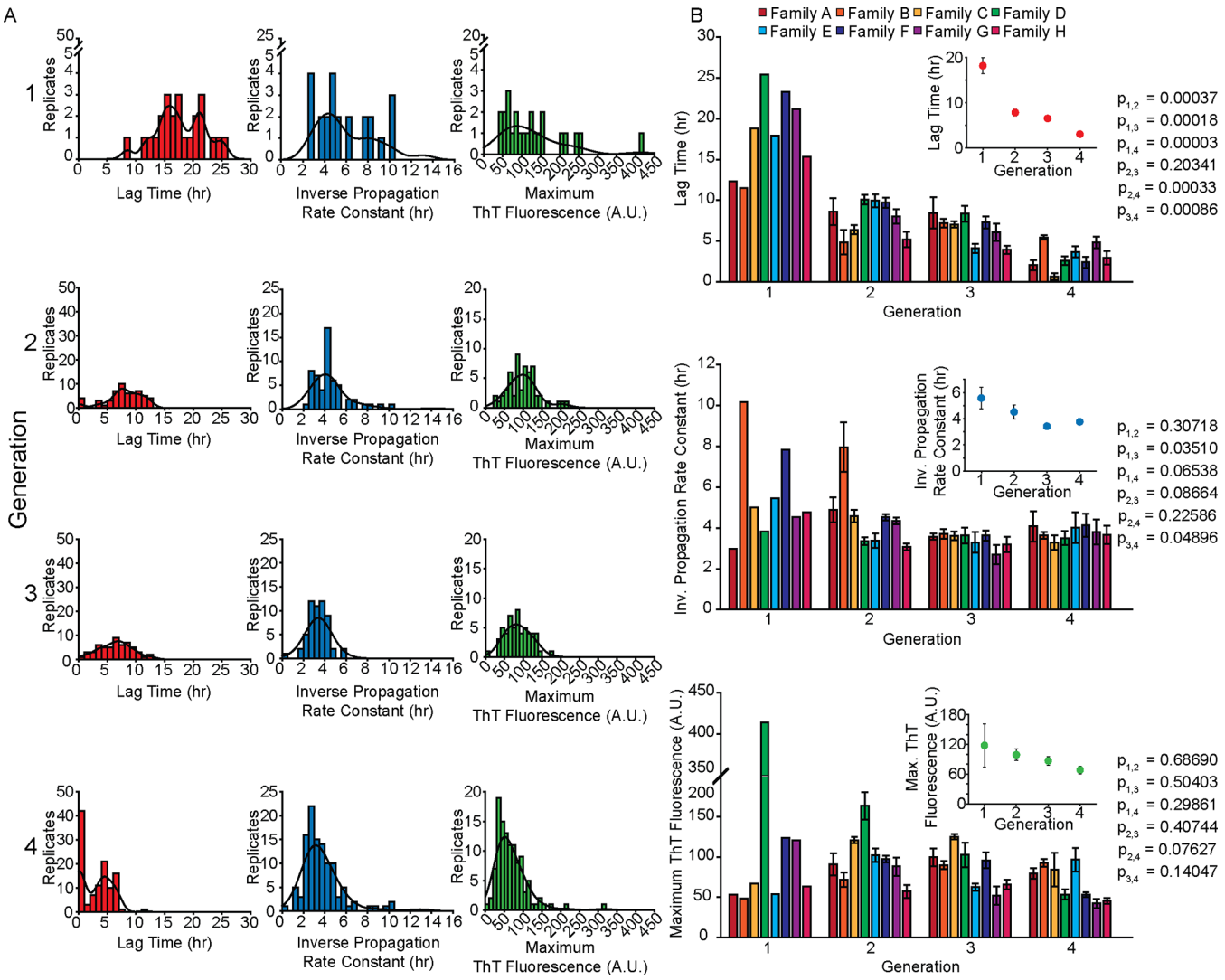

Figure 4. Comparison of lag time, inverse propagation rate constant, and maximum ThT fluorescence of fibrils formed across four generations (unseeded parent fibrils to great granddaughter fibrils). (A) Distributions of lag time, inverse propagation rate constant, and maximum ThT fluorescence for each generation of eight discrete families of aggregates. Generation 1 distributions include all 24 replicates. (B) Mean values of lag time, inverse propagation rate constant, and maximum ThT fluorescence for each generation of eight discrete families of aggregates (from Figure 3). Error bars represent standard error of the mean. *P* values comparing different generations were calculated using an unpaired Student's *t* test and include the averages of all replicates of each family in a given generation.

generation fibrillization in a given family varied by only ∼7 h (on average) compared to ∼14 h variation for progenitor fibrils. The inverse propagation rate constant varied by ∼3 h (on average) in a given family of second-generation fibrils (the inverse propagation rate constant of first-generation fibrils varied by ∼7 h). This expected result likely occurs because the nucleation step is bypassed in seeded fibrillization.

Second-generation fibrils formed at approximately similar rates regardless of the rate of formation of the parent seed (Figure 4B). For example, the parent fibril of family A formed with a lag time of 12.31 h and an inverse propagation rate constant of 2.96 h, the daughter fibrils formed with a mean lag time of 8.61 ± 1.63 h and a mean inverse propagation rate constant of 4.89 ± 0.62 h (Figure 4B). The parent fibril of family C formed with a lag time of 18.80 h and an inverse propagation rate constant of 5.01 h, while the daughter fibrils, however, formed at rates statistically indistinguishable from that of family A (lag = 6.39 ± 0.58 h, p = 0.22; inverse propagation = 4.58 ± 0.31 h; p = 0.65) (Figure 4B). This result suggests to us that the types of amyloid fibrils that form in unseeded assays are similar and that only their rate of formation varies (is stochastic), possibly due to competing pathways of amorphous aggregation.

The observed decrease in stochasticity is due to not only the exogenous seed but also a direct result of the shorter lag time associated with seeded fibrillization. Fibrillization processes that occur rapidly during microplate assays will have less measurable variation than slower fibrillization processes. For example, in the case of SOD1, previous studies used different types of 3.2 mm beads to decrease the lag time and variation of unseeded fibrillization of SOD1. In these experiments, heavier beads (e.g., steel) produced shorter lag times with less stochasticity than lighter beads (acrylic) with the distribution of lag times decreasing from 17.8 ± 1.4 h (acrylic) to 3.7 ± 0.1 h (steel).[18]

Generational Differences in ThT Fluorescence. Previous studies have shown that the stochastic fibrillization of SOD1 not only manifests in variation in observed lag time and

https://dx.doi.org/10.1021/acschemneuro.9b00464
ACS Chem. Neurosci. 2020, 11, 304−313

propagation rate but also in the maximal ThT fluorescence reached during an iterate assay.[13,17] In this study, and previous studies,[13,17] the maximum ThT fluorescence of iterate assays of unseeded WT fibrillization varied 10-fold from well to well, typically ranging from 40 to 400 A.U. (Figures 1B, 3, and 4). Understanding this variation in fluorescence is important because there is a weak correlation between ThT fluorescence of ALS mutant SOD1 fibrils formed *in vitro* and clinical phenotype of the ALS-linked SOD1 mutation in ALS patients (in one study, lower fluorescence correlated with a more severe phenotype).[8] The source of the variation in fluorescence is not understood and could reflect differences in (i) binding stoichiometry of ThT to different types of fibrils; (ii) differences in fluorescence quantum yield; or (iii) differences in concentration of fibrils in each iterate well (caused by off pathway aggregation to nonfibrillar species). These three outcomes are not mutually exclusive.

We found that although the fluorescence of the first-generation fibrils varied 10-fold across families, the progeny fibrils produced at each generation were more similar in fluorescence across families (~100−150 A.U.), regardless of the fluorescence of the parent fibril (Figure 4B). This result suggests that the types of first-generation progenitor fibrils formed in each population (microplate well) of SOD1 are similar, that is, produce similar progeny fibrils and that the differences in lag time, propagation rate, and maximal ThT fluorescence of first-generation parent fibrils might be caused by differences in the concentration of fibrils in each well. The morphology of progenitor and progeny fibrils was grossly similar according to transmission electron microscopy (Figure 5). For example, all families exhibited structures with both amorphous and fibrillar morphology, however, family D (gen 1) exhibited more fibrillar morphology (and the highest maximum ThT Fluorescence) (Figure 5). As in previous studies, we hypothesize that iterate wells of identical solutions of SOD1 produce different concentrations of unseeded progenitor fibrils via competition between amorphous aggregation and fibrillization.[17] Nevertheless, why do these variations in fibrillization cease or become less pronounced upon seeding for the second generation and beyond? The simplest explanation is that the initial formation of amorphous and fibrillar nuclei in the original parent solution might occur at rates that are similar in their order of magnitude such that these two pathways compete for native protein. Assuming that the propagation of amyloid fibrils is, however, much faster than the propagation of amorphous species under these conditions, then fibrils would be the consistent product when mixtures of preformed amorphous and fibrillar seeds (progenitor solutions) are added to native protein (regardless of differences in the initial concentration of amorphous or fibrillar species in the solution used as a seed).

The apparent increase in the maximum ThT fluorescence of SOD1 fibrillization, after iterative seeding of SOD1 with low ThT-positive wells, is reminiscent of the general effect of iterative crystal seeding in protein crystallography, where the quality of protein crystals can be improved by iterative seeding.[38] This is also the case for populations of fibrillar SOD1—albeit a 2D crystal instead of a 3D crystal—in which the lag time continues to decrease from one generation to the next. However, with amyloid seeding of SOD1, we note that the increase in ThT-positive fibrils halts after the third generation, whereby the fourth-generation fibrils of some families (e.g., family D) have low ThT fluorescence. (Figure 3, 4B) Similarly, the amount of noise observed in ThT fluorescence assays increases between generations three and four (Figure 3), possibly resulting in artificially low lag times observed in generation four (this effect was greater for some families than others). This diminished seeding ability of third-generation fibrils suggests that there is a limit or lifetime to the number of seeding iterations that can be performed on pure SOD1 in a nonquiescent microplate assay. The cause of this finite lifetime is not known but could result from the buildup of amorphous aggregates across multiple generations, or some other polymorph of aggregated SOD1 that impairs (that "poisons")[39,40] the formation of ThT-positive fibrils. We cannot exclude unidentified experimental artifacts as being the cause of this generational decay in seeding ability, however, we note that each iterative amyloid assay involved freshly thawed aliquots of SOD1 protein and fresh solutions of ThT and other reagents, which were filtered prior to use. We note that lifetimes for iterative seeding and "self-poisoning" have been observed for 3D crystals of small molecules and colloids.[39,40]

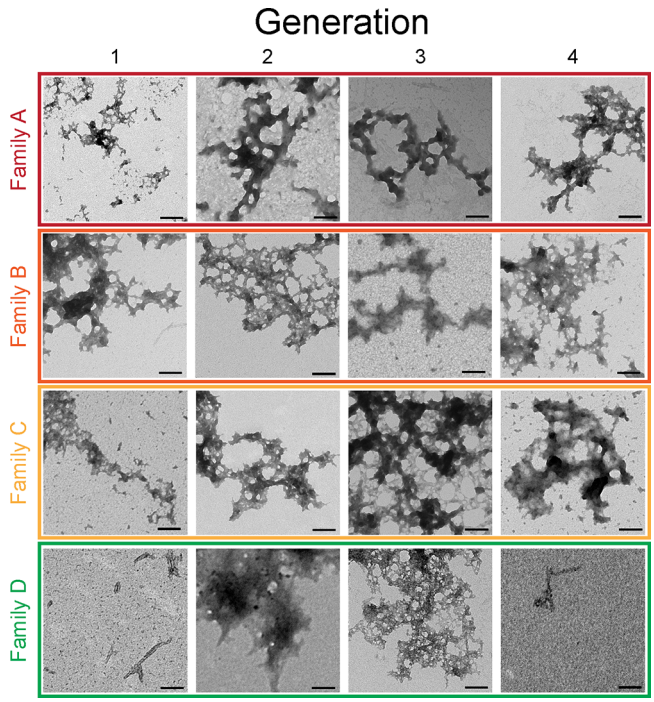

Figure 5. Morphology of aggregated SOD1 across multiple generations. Transmission electron micrographs of aggregates resulting from four families of generational aggregation assays (labels and colors correspond to plots in Figure 3). Scale bars represent 100 nm. The progenitor and progeny fibrils shown here represent the full range of lag time, inverse propagation rate constant, and maximum ThT fluorescence.

Concentration Dependence of Fibrillization. The propagation rate of seeded fibrillization of SOD1 was dependent on monomer concentration and weakly dependent on fibril (i.e., seed) concentration (Figure 6). Monomer concentration varied from 30 to 120 μM (monomeric) SOD1 and seed concentration varied from 2.5 to 20% (v/v), resulting in propagation rates ranging from ~1 h^{-1} (at 30 μM SOD1, 2.5% seed) to ~30 h^{-1} (at 90 μM SOD1, 20% seed and 120 μM SOD1, 10% or 20% seed) (Figure 6). A 10-fold increase in apparent propagation rate was observed when monomer concentration was increased 4-fold, whereas a 4-fold increase

https://dx.doi.org/10.1021/acschemneuro.9b00464
ACS Chem. Neurosci. 2020, 11, 304−313

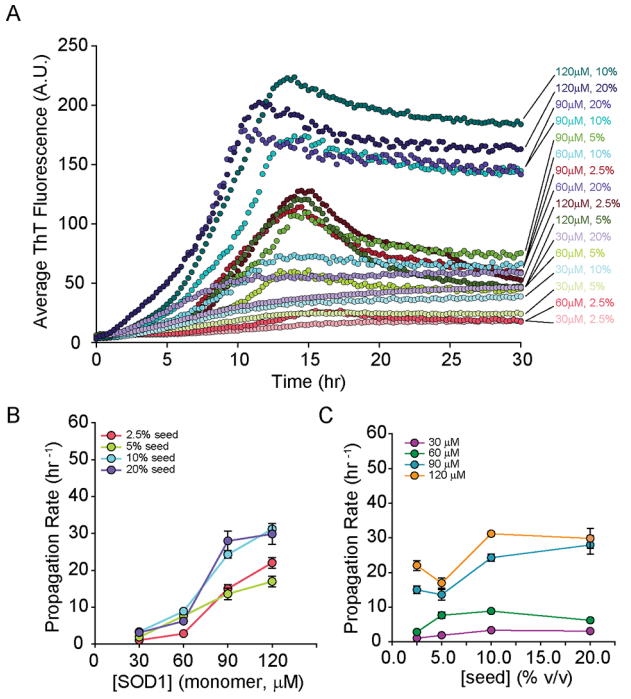

Figure 6. Concentration dependence of apparent propagation rate of SOD1 fibrillization. (A) Fibrillization of 30, 60, 90, or 120 μM SOD1 (monomer) initiated by the addition of a 2.5, 5, 10, or 20% (v/v) seed was monitored via ThT fluorescence. Traces of ThT fluorescence are representative of the average of seven replicates. (B) Change in apparent propagation rate with respect to increasing concentration of SOD1 and (C) increasing concentration of seed. The apparent propagation rate was determined from the first derivative of each replicate individually and then averaged, rather than determining the apparent propagation rate from the average curve. Error bars represent the standard error of the mean.

in seed concentration only increased the apparent propagation rate ~3-fold. Data could not be perfectly fit to any classical rate laws applied to amyloid fibrillization,[41−44] in part because the exact relationship between ThT fluorescence intensity and SOD1 fibril concentration is not known. However, our data most closely fit rate laws associated with monomer-dependent secondary nucleation and elongation, as expected.[41,44] In this case, $v_{prop} = k_{prop}[f][SOD1]^n$ (where [f] = concentration of fibril seed upon which a nucleus forms, and n = the number of SOD1 monomers in the critical nucleus). Interestingly, the lowest seed concentration (2.5%) with high concentrations of SOD1 yielded fibrillization kinetics with faster propagation than those of identical SOD1 concentration but double the seed concentration (5%). This effect was not observed when seed concentration was increased to 10% or 20%.

CONCLUSION

The results of this study provide some practical guidelines for carrying out *in vitro* seeding assays of SOD1 fibrillization. For example, because progenitor fibrils of SOD1 form stochastically in microplate assays, multiple replicates (ideally n = 100) would normally be required in any type of experiment that sought to obtain average rates of aggregation that are statistically significant.[17] However, daughter (progeny) fibrils form at similar rates (with a narrower distribution of rates than progenitor fibrils), regardless of the rate at which parent fibrils formed. Therefore, solutions of amyloid seeds that might be used for seeding experiments are not required to be pooled from kinetically representative solutions of first-generation parent fibrils. In addition, whereas the ThT fluorescence of parent fibrils can vary by an order of magnitude, the ThT fluorescence of daughter fibrils are more similar, regardless of the ThT fluorescence of the parent fibril that was used as a seed.

These results suggest that the disparate fluorescence and lag times of different populations (wells) of SOD1 are not caused by inherently different types or "strains" of fibrils, but rather by different concentrations of fibrillar versus amorphous aggregates (note that some studies suggest that SOD1-linked ALS is a non-amyloid disease caused principally by amorphous aggregates).[45] What can the results of microplate amyloid assays for SOD1 tell us about the fibrillization of SOD1 in discrete populations of SOD1 *in vivo*, that is, in neural cells? First and foremost, the stochastic aggregation of SOD1 in a population of cells would result in variable concentrations of different types of aggregates, for example, mixtures of different amorphous and fibrillar species with cell-to-cell variation in concentration of each species. The results of this study suggest that the formation rate and concentration of progenitor fibrils in one cell will not be the only factor determining the seeding rate or seeding propensity of those fibrils in neighboring cells or in extracellular space and that rate will also be dependent upon the concentration of native SOD1 or monomers of SOD1 in neighboring cells or extracellular environments.

The overarching question of nearly every result described in this paper is why? Why is the aggregation of SOD1 (into amorphous or fibrillar species) stochastic? Why do slow and fast forming progenitor fibrils both produce daughter fibrils at similar rates? Answering these questions with certainty will likely require a detailed atomic or morphological characterization and quantitation of assemblies present in the iterate solutions of progenitor and progeny fibrils (and amorphous aggregates) and determination of their respective rates of formation. For now, these data can be rationalized by comparison to classical rate laws for amyloid fibrillization.[41,44] Our data suggested that monomer-dependent secondary nucleation is the dominant mechanism under our conditions and propagation rate is more dependent upon monomer concentration than fibril concentration (at the concentrations studied) (Figure 6).[41,44] Such rate laws, assuming $n \gg 1$ for SOD1 (n = nucleus stoichiometry), can begin to explain why two wells (or cells) with differences in the concentration of fibrillar SOD1 will seed the fibrillization of native SOD1 at roughly similar rates.

METHODS

Purification and Demetalation of SOD1. Wild-type SOD1 was recombinantly overexpressed in *Saccharomyces cerevisiae* and purified using successive ammonium sulfate precipitation, hydrophobic interaction chromatography, ion exchange chromatography, and size exclusion chromatography, as previously described.[46] Resulting protein solution was verified to contain SOD1 via SDS-PAGE following each chromatographic step of purification. Purity was verified via mass spectrometry (Synapt G2, Waters). Once purified, SOD1 was demetalated via sequential dialysis in (i) 0.1 M sodium acetate, 10 mM EDTA pH 3.8, (ii) 0.1 M sodium acetate, 10 mM NaCl pH 3.8, and (iii) 0.1 M sodium acetate pH 5.5. Full demetalation of SOD1 was verified with inductively coupled plasma-mass spectrometry (7900 ICP-MS, Agilent Technologies). Fully demetalated SOD1 was aliquoted into cryogenic microcentrifuge tubes, flash frozen, and stored at −80 °C until use.

https://dx.doi.org/10.1021/acschemneuro.9b00464
ACS Chem. Neurosci. 2020, 11, 304−313

ThT Fluorescence Aggregation Assays. Thioflavin-T (ThT) fluorescence aggregation assays were carried out in a black nonbinding surface polystyrene 96-well microplate (Corning) and were monitored using a Fluoroskan Ascent FL microplate fluorometer (Thermo Scientific). Briefly, apo-WT SOD1, Tris(2-carboxyethyl)-phosphine (TCEP), and ThT were combined in aggregation buffer (10 mM potassium phosphate, 5 mM EDTA, pH 7.4) to the following final concentrations (for typical assays): $[SOD1]_{dimer}$= 30 μM; [TCEP] = 10 mM; [ThT] = 20 μM. All components except for ThT were mixed and allowed to incubate at room temperature for 30 min. Following the incubation period, ThT was added to the solution, and the entire solution was filtered using a 0.2 μm syringe filter. For unseeded assays, 100 μL, 200 μL, or 330 μL of this solution was administered to each well (depending on the desired headspace volume), and for seeded assays, 180 μL of this solution was administered to each well, followed by 20 μL of fibril seed solution. For assays to determine the concentration dependence of the propagation rate, final SOD1 concentration was 30, 60, 90, or 120 μM (monomer), and seed concentration was 2.5, 5, 10, or 20% (by volume) (see Preparation of Fibril Seeds). Each of these reactions (in a single microplate well) had a final volume of 200 μL and contained a Teflon bead (white, d = 3.13 mm). An adhesive seal was gently heated and immediately placed on top of the microplate. During analysis, the microplate was incubated at 37 °C and was subjected to intermittent gyration (15 s on, 15 s off) at 360 rpm. A fluorescence measurement was recorded every 15 min for at least 60 h.

Preparation of Fibril Seeds. Upon completion of a ThT fluorescence aggregation assay (at 30 μM SOD1 dimer, 200 μL total volume), well contents were removed from the 96-well microplate and transferred to a 1.5 mL microcentrifuge tube. Aggregates which were attached to the edges of their microplate well were carefully removed by gently pipetting the well contents and lightly scratching the sides of the well with the pipet tip. For first-generation assays, each well was kept separate from one another, and for generations 2–4, each of the 7 replicates in a given family were pooled to create a single seed solution to be used in the next generation. The resulting seeds were washed immediately prior to use as to remove excess ThT. This was accomplished by centrifugation at 17,000g for 20 min at 4 °C, followed by removal of the supernatant. The volume removed was then replaced with fresh 10 mM phosphate, 5 mM EDTA buffer pH 7.4, and the pellet was resuspended. Centrifugation was repeated until pellet was mostly white in color (rather than yellow, indicating the presence of ThT). Upon completion, the pellets were resuspended, flash frozen, and stored at −80 °C until use. For assays in which seed concentration was varied intentionally, the seed fibrils were grown for 5 days as described above, except that there was no ThT. At the end of 5 days, aggregates from 18 replicate wells were pooled into a single seed solution and represent the full kinetic spectra of progenitor fibrils.

Curve Fitting and Analysis of Aggregation Assay Data. All aggregation assay data were plotted and analyzed using SigmaPlot 14.0 (Systat). Briefly, data was plotted as ThT fluorescence versus time and the resulting curve was fit to a 4-parameter sigmoid using the equation below with weight given to reciprocal y. Lag time and inverse propagation rate constant were calculated from the resulting sigmoid where lag time = $x_0 - 2b$ and inverse propagation rate constant = b. Statistical significance of comparisons was determined with an unpaired Student's t test.

$$f = y_0 + \frac{a}{(1 + e^{-x-x_0/b})}$$

Data resulting from assays in which monomer and seed concentration were deliberately varied were not curve fit because many replicates (including those at very high seed concentration) could not be adequately fit to the 4-parameter sigmoid we typically use to curve fit. Instead, the apparent propagation rate was determined from the value of the first derivative at the inflection point of the curve.

Transmission Electron Microscopy. Aggregates of SOD1 were imaged and their morphology analyzed using a JEOL JEM-1010 high contrast transmission electron microscope operating at 60 kV. Images were captured with an XR16 CCD camera attached to the microscope. Sample preparation was performed by incubating a copper grid on ∼10 μL of each the following solutions: (i) SOD1 fibril solution (150 s), (ii) 10 mM phosphate buffer, pH 7.4 (twice, 150 s each), (iii) 3% uranyl acetate (5 s). After staining with uranyl acetate, excess liquid was wicked away with filter paper, and the grid was returned to a dust-free chamber to dry overnight prior to imaging.

AUTHOR INFORMATION

Corresponding Author

Bryan F. Shaw − *Baylor University, Waco, Texas;*
orcid.org/0000-0001-8265-5833;
Email: bryan_shaw@baylor.edu

Other Authors

Katelyn M. Baumer − *Baylor University, Waco, Texas;*
orcid.org/0000-0003-2364-8136

Jordan C. Koone − *Baylor University, Waco, Texas;*
orcid.org/0000-0003-2021-5298

Complete contact information is available at:
https://pubs.acs.org/10.1021/acschemneuro.9b00464

Author Contributions

K.M.B. performed the experiments. K.M.B. and B.F.S. analyzed data and wrote and edited the manuscript. J.C.K. purified protein for use in the experiments.

Funding

This research was supported by grants from the National Science Foundation (CHE: 1856449, CHE: 1352122) and the Welch Foundation (AA-1854).

Notes

The authors declare no competing financial interest.

ACKNOWLEDGMENTS

The authors would like to thank the Center for Microscopy and Imaging at Baylor University for technical support during microscopy and image analysis.

REFERENCES

(1) Nardo, G., Trolese, M. C., Tortarolo, M., Vallarola, A., Freschi, M., Pasetto, L., Bonetto, V., and Bendotti, C. (2016) New insights on the mechanisms of disease course variability in ALS from mutant SOD1 mouse models. *Brain Pathol. 26* (2), 237–47.

(2) Silverman, J. M., Fernando, S. M., Grad, L. I., Hill, A. F., Turner, B. J., Yerbury, J. J., and Cashman, N. R. (2016) Disease mechanisms in ALS: misfolded SOD1 transferred through exosome-dependent and exosome-independent pathways. *Cell. Mol. Neurobiol. 36* (3), 377–81.

(3) van Zundert, B., and Brown, R. H., Jr (2017) Silencing strategies for therapy of SOD1-mediated ALS. *Neurosci. Lett. 636*, 32–9.

(4) Ayers, J. I., Fromholt, S. E., O'Neal, V. M., Diamond, J. H., and Borchelt, D. R. (2016) Prion-like propagation of mutant SOD1 misfolding and motor neuron disease spread along neuroanatomical pathways. *Acta Neuropathol. 131* (1), 103–14.

(5) Come, J. H., Fraser, P. E., and Lansbury, P. T. (1993) A kinetic model for amyloid formation in the prion diseases: importance of seeding. *Proc. Natl. Acad. Sci. U. S. A. 90* (13), 5959–63.

(6) Pokrishevsky, E., Grad, L. I., and Cashman, N. R. (2016) TDP-43 or FUS-induced misfolded human wild-type SOD1 can propagate intercellularly in a prion-like fashion. *Sci. Rep. 6*, 22155.

(7) Chattopadhyay, M., Durazo, A., Sohn, S. H., Strong, C. D., Gralla, E. B., Whitelegge, J. P., and Valentine, J. S. (2008) Initiation and elongation in fibrillation of ALS-linked superoxide dismutase. *Proc. Natl. Acad. Sci. U. S. A. 105* (48), 18663–8.

(8) Abdolvahabi, A., Shi, Y., Rasouli, S., Croom, C. M., Aliyan, A., Marti, A. A., and Shaw, B. F. (2017) Kaplan-Meier meets chemical

kinetics: intrinsic rate of SOD1 amyloidogenesis decreased by subset of ALS mutations and cannot fully explain age of disease onset. *ACS Chem. Neurosci. 8* (6), 1378−89.
(9) Wang, Q., Johnson, J. L., Agar, N. Y., and Agar, J. N. (2008) Protein aggregation and protein instability govern familial amyotrophic lateral sclerosis patient survival. *PLoS Biol. 6* (7), No. e170.
(10) Israelson, A., Arbel, N., Da Cruz, S., Ilieva, H., Yamanaka, K., Shoshan-Barmatz, V., and Cleveland, D. W. (2010) Misfolded mutant SOD1 directly inhibits VDAC1 conductance in a mouse model of inherited ALS. *Neuron 67* (4), 575−87.
(11) Magri, A., Belfiore, R., Reina, S., Tomasello, M. F., Di Rosa, M. C., Guarino, F., Leggio, L., De Pinto, V., and Messina, A. (2016) Hexokinase I N-terminal based peptide prevents the VDAC1-SOD1 G93A interaction and re-establishes ALS cell viability. *Sci. Rep. 6*, 34802.
(12) Wright, G. S., Antonyuk, S. V., and Hasnain, S. S. (2016) A faulty interaction between SOD1 and hCCS in neurodegenerative disease. *Sci. Rep. 6*, 27691.
(13) Rasouli, S., Abdolvahabi, A., Croom, C. M., Plewman, D. L., Shi, Y., and Shaw, B. F. (2018) Glycerolipid headgroups control rate and mechanism of superoxide dismutase-1 aggregation and accelerate fibrillization of slowly aggregating amyotrophic lateral sclerosis mutants. *ACS Chem. Neurosci. 9* (7), 1743−56.
(14) Ahtoniemi, T., Jaronen, M., Keksa-Goldsteine, V., Goldsteins, G., and Koistinaho, J. (2008) Mutant SOD1 from spinal cord of G93A rats is destabilized and binds to inner mitochondrial membrane. *Neurobiol. Dis. 32* (3), 479−85.
(15) Lim, L., Lee, X., and Song, J. (2015) Mechanism for transforming cytosolic SOD1 into integral membrane proteins of organelles by ALS-causing mutations. *Biochim. Biophys. Acta, Biomembr. 1848*, 1−7.
(16) Watanabe, S., Ilieva, H., Tamada, H., Nomura, H., Komine, O., Endo, F., Jin, S., Mancias, P., Kiyama, H., and Yamanaka, K. (2016) Mitochondria-associated membrane collapse is a common pathomechanism in SIGMAR1- and SOD1-linked ALS. *EMBO Mol. Med. 8* (12), 1421−37.
(17) Abdolvahabi, A., Shi, Y., Chuprin, A., Rasouli, S., and Shaw, B. F. (2016) Stochastic formation of fibrillar and amorphous superoxide dismutase oligomers linked to amyotrophic lateral sclerosis. *ACS Chem. Neurosci. 7* (6), 799−810.
(18) Abdolvahabi, A., Shi, Y., Rasouli, S., Croom, C. M., Chuprin, A., and Shaw, B. F. (2017) How do gyrating beads accelerate amyloid fibrillization? *Biophys. J. 112* (2), 250−64.
(19) Atlasi, R. S., Malik, R., Corrales, C. I., Tzeplaeff, L., Whitelegge, J. P., Cashman, N. R., and Bitan, G. (2018) Investigation of anti-SOD1 antibodies yields new structural insight into SOD1 misfolding and surprising behavior of the antibodies themselves. *ACS Chem. Biol. 13* (9), 2794−807.
(20) Shi, Y., Rhodes, N. R., Abdolvahabi, A., Kohn, T., Cook, N. P., Marti, A. A., and Shaw, B. F. (2013) Deamidation of asparagine to aspartate destabilizes Cu, Zn superoxide dismutase, accelerates fibrillization, and mirrors ALS-linked mutations. *J. Am. Chem. Soc. 135* (42), 15897−908.
(21) Malik, R., Meng, H., Wongkongkathep, P., Corrales, C. I., Sepanj, N., Atlasi, R. S., Klarner, F. G., Schrader, T., Spencer, M. J., Loo, J. A., Wiedau, M., and Bitan, G. (2019) The molecular tweezer CLR01 inhibits aberrant superoxide dismutase 1 (SOD1) self-assembly in vitro and in the G93A-SOD1 mouse model of ALS. *J. Biol. Chem. 294* (10), 3501−13.
(22) Lang, L., Zetterstrom, P., Brannstrom, T., Marklund, S. L., Danielsson, J., and Oliveberg, M. (2015) SOD1 aggregation in ALS mice shows simplistic test tube behavior. *Proc. Natl. Acad. Sci. U. S. A. 112* (32), 9878−83.
(23) Eugene, S., Xue, W. F., Robert, P., and Doumic, M. (2016) Insights into the variability of nucleated amyloid polymerization by a minimalistic model of stochastic protein assembly. *J. Chem. Phys. 144* (17), 175101.
(24) Hortschansky, P., Schroeckh, V., Christopeit, T., Zandomeneghi, G., and Fandrich, M. (2005) The aggregation kinetics of Alzheimer's beta-amyloid peptide is controlled by stochastic nucleation. *Protein Sci. 14* (7), 1753−9.
(25) Blancas-Mejia, L. M., and Ramirez-Alvarado, M. (2016) Recruitment of light chains by homologous and heterologous fibrils shows distinctive kinetic and conformational specificity. *Biochemistry 55* (21), 2967−78.
(26) Campioni, S., Carret, G., Jordens, S., Nicoud, L., Mezzenga, R., and Riek, R. (2014) The presence of an air-water interface affects formation and elongation of alpha-Synuclein fibrils. *J. Am. Chem. Soc. 136* (7), 2866−75.
(27) Hu, K. N., McGlinchey, R. P., Wickner, R. B., and Tycko, R. (2011) Segmental polymorphism in a functional amyloid. *Biophys. J. 101* (9), 2242−50.
(28) Petkova, A. T., Leapman, R. D., Guo, Z., Yau, W. M., Mattson, M. P., and Tycko, R. (2005) Self-propagating, molecular-level polymorphism in Alzheimer's beta-amyloid fibrils. *Science 307* (5707), 262−5.
(29) Tycko, R. (2014) Physical and structural basis for polymorphism in amyloid fibrils. *Protein Sci. 23* (11), 1528−39.
(30) Tycko, R. (2015) Amyloid polymorphism: structural basis and neurobiological relevance. *Neuron 86* (3), 632−45.
(31) Andersen, C. B., Yagi, H., Manno, M., Martorana, V., Ban, T., Christiansen, G., Otzen, D. E., Goto, Y., and Rischel, C. (2009) Branching in amyloid fibril growth. *Biophys. J. 96* (4), 1529−36.
(32) Pedersen, J. S., Andersen, C. B., and Otzen, D. E. (2010) Amyloid structure–one but not the same: the many levels of fibrillar polymorphism. *FEBS J. 277* (22), 4591−601.
(33) Silverman, J. M., Christy, D., Shyu, C. C., Moon, K. M., Fernando, S., Gidden, Z., Cowan, C. M., Ban, Y., Stacey, R. G., Grad, L. I., McAlary, L., Mackenzie, I. R., Foster, L. J., and Cashman, N. R. (2019) CNS-derived extracellular vesicles from superoxide dismutase 1 (SOD1)(G93A) ALS mice originate from astrocytes and neurons and carry misfolded SOD1. *J. Biol. Chem. 294* (10), 3744−59.
(34) Grad, L. I., and Cashman, N. R. (2014) Prion-like activity of Cu/Zn superoxide dismutase: implications for amyotrophic lateral sclerosis. *Prion 8* (1), 33−41.
(35) Clarke, G., Collins, R. A., Leavitt, B. R., Andrews, D. F., Hayden, M. R., Lumsden, C. J., and McInnes, R. R. (2000) A one-hit model of cell death in inherited neuronal degenerations. *Nature 406* (6792), 195−9.
(36) Rosen, D. R., Siddique, T., Patterson, D., Figlewicz, D. A., Sapp, P., Hentati, A., Donaldson, D., Goto, J., O'Regan, J. P., Deng, H. X., Rahmani, Z., Krizus, A., McKenna-Yasek, D., Cayabyab, A., Gaston, S. M., Berger, R., Tanzi, R. E., Halperin, J. J., Herzfeldt, B., Van den Bergh, R., Hung, W. Y., Bird, T., Deng, G., Mulder, D. W., Smyth, C., Laing, N. G., Soriano, E., Paricak-Vance, M. A., Haines, J., Rouleau, G. A., Gusella, J. S., Horvitz, H. R., and Brown, R. H. (1993) Mutations in Cu/Zn superoxide dismutase gene are associated with familial amyotrophic lateral sclerosis. *Nature 362*, 59−62.
(37) Gade Malmos, K., Blancas-Mejia, L. M., Weber, B., Buchner, J., Ramirez-Alvarado, M., Naiki, H., and Otzen, D. (2017) ThT 101: a primer on the use of thioflavin T to investigate amyloid formation. *Amyloid 24* (1), 1−16.
(38) D'Arcy, A., Bergfors, T., Cowan-Jacob, S. W., and Marsh, M. (2014) Microseed matrix screening for optimization in protein crystallization: what have we learned? *Acta Crystallogr., Sect. F: Struct. Biol. Commun. 70*, 1117−1126.
(39) Allahyarov, E., Sandomirski, K., Egelhaaf, S. U., and Lowen, H. (2015) Crystallization seeds favour crystallization only during initial growth. *Nat. Commun. 6*, 7110.
(40) Bergfors, T. (2003) Seeds to crystals. *J. Struct. Biol. 142* (1), 66−76.
(41) Arosio, P., Knowles, T. P., and Linse, S. (2015) On the lag phase in amyloid fibril formation. *Phys. Chem. Chem. Phys. 17* (12), 7606−18.
(42) Meisl, G., Kirkegaard, J. B., Arosio, P., Michaels, T. C., Vendruscolo, M., Dobson, C. M., Linse, S., and Knowles, T. P. (2016) Molecular mechanisms of protein aggregation from global fitting of kinetic models. *Nat. Protoc. 11* (2), 252−72.

(43) Michaels, T. C. T., Saric, A., Habchi, J., Chia, S., Meisl, G., Vendruscolo, M., Dobson, C. M., and Knowles, T. P. J. (2018) Chemical Kinetics for Bridging Molecular Mechanisms and Macroscopic Measurements of Amyloid Fibril Formation. *Annu. Rev. Phys. Chem. 69*, 273−298.
(44) Murphy, R. M. (2007) Kinetics of amyloid formation and membrane interaction with amyloidogenic proteins. *Biochim. Biophys. Acta, Biomembr. 1768* (8), 1923−34.
(45) Kerman, A., Liu, H. N., Croul, S., Bilbao, J., Rogaeva, E., Zinman, L., Robertson, J., and Chakrabartty, A. (2010) Amyotrophic lateral sclerosis is a non-amyloid disease in which extensive misfolding of SOD1 is unique to the familial form. *Acta Neuropathol. 119* (3), 335−44.
(46) Shi, Y., Mowery, R. A., and Shaw, B. F. (2013) Effect of metal loading and subcellular pH on net charge of superoxide dismutase-1. *J. Mol. Biol. 425* (22), 4388−404.
(47) Abdolvahabi, A., Shi, Y., Rhodes, N. R., Cook, N. P., Marti, A. A., and Shaw, B. F. (2015) Arresting amyloid with coulomb's law: acetylation of ALS-linked SOD1 by aspirin impedes aggregation. *Biophys. J. 108* (5), 1199−212.

https://dx.doi.org/10.1021/acschemneuro.9b00464
ACS Chem. Neurosci. 2020, 11, 304−313